Available online at www.sciencedirect.com

ScienceDirect

Ceramics International 42 (2016) 4107–4119

CERAMICS INTERNATIONAL

www.elsevier.com/locate/ceramint

Effect of oxygen flow rate on the ultraviolet sensing properties of zinc oxide nanocolumn arrays grown by radio frequency magnetron sputtering

M.H. Mamat[a,b,*], M.F. Malek[a,b], N.N. Hafizah[b], M.N. Asiah[b], A.B. Suriani[c], A. Mohamed[c], N. Nafarizal[d], M.K. Ahmad[d], M. Rusop[a,b]

[a]*NANO-ElecTronic Centre (NET), Faculty of Electrical Engineering, Universiti Teknologi MARA (UiTM), 40450 Shah Alam, Selangor, Malaysia*
[b]*NANO-SciTech Centre (NST), Institute of Science (IOS), Universiti Teknologi MARA (UiTM), 40450 Shah Alam, Selangor, Malaysia*
[c]*Nanotechnology Research Centre, Faculty of Science and Mathematics, Universiti Pendidikan Sultan Idris (UPSI), 35900 Tanjung Malim, Perak, Malaysia*
[d]*Microelectronic and Nanotechnology–Shamsuddin Research Centre (MiNT-SRC), Faculty of Electrical and Electronic Engineering, Universiti Tun Hussein Onn Malaysia (UTHM), 86400 Batu Pahat, Johor, Malaysia*

Received 17 September 2015; received in revised form 15 November 2015; accepted 16 November 2015
Available online 22 November 2015

Abstract

Highly transparent metal–semiconductor–metal ultraviolet (UV) photoconductive sensors were fabricated using thin (less than 100 nm in thickness), dense, small-diameter ZnO nanocolumn arrays prepared via low-power, catalyst-free radio frequency (RF) magnetron sputtering at different oxygen flow rates ranging from 0 to 25 sccm. The FESEM images revealed the average nanocolumn diameter decreased with increasing oxygen flow rate. The transmittance spectra show that with the introduction of oxygen, the transmittance of the nanocolumn arrays in the visible region improves relative to that of a film prepared in the absence of oxygen with values greater than 95%. The UV responsivity and sensitivity were significantly improved for sputtered ZnO nanocolumn arrays prepared at oxygen flow rates up to 10 sccm, with the highest values of 9.70 mA/W and 2.20×10^4. Furthermore, the responsivity and sensitivity decreased at oxygen flow rates greater than 10 sccm, which can be attributed to the increased electrical resistance of the nanocolumn arrays. Our findings indicate that a high-performance UV photoconductive sensor can be realised using very thin sputtered ZnO nanocolumn arrays and that such a sensor would exhibit high sensitivity.

Keywords: D. ZnO; Nanocolumn arrays; RF magnetron sputtering; UV photoconductive sensor; Oxygen flow rate

---

1. Introduction

Nanostructured zinc oxide (ZnO) has emerged as a promising material for applications in UV photoconductive sensors because of its unique physical and chemical characteristics, wide bandgap energy of 3.3 eV, and high exciton binding energy of 60 meV. Nanostructured ZnO-based UV photoconductive sensors have been widely studied because of their numerous applications, which include gas sensors, surface acoustic wave (SAW) devices, flame sensors, and ozone monitoring. Various ZnO nanostructures have been studied for UV photoconductive sensor applications, including nanofibers [1], nanoflakes [2], nanosheets [3], and nanorods [4–7]. The performance of UV photoconductive sensors has been significantly improved through the use of ZnO one-dimensional (1D) nanostructured arrays, in particular, because of the characteristics of the 1D nanostructured arrays, which have a high surface-to-volume ratio and high electron mobility. Numerous synthesis methods have been reported for the preparation ZnO 1D nanostructured arrays, including vapour solid deposition [8], electrodeposition [9,10], metal–organic chemical vapour deposition (MOCVD) [11], pulsed laser deposition (PLD) [12], and solution-based processes [13–17]. The preparation of ZnO 1D nanostructured arrays using a sputtering process is important in the fabrication of devices because of this method's advantages, which include a low deposition temperature, the possibility of large-scale synthesis, and the relatively low cost compared with that of other vacuum-

---

[*] Corresponding author. Tel.: +60 3 55211883; fax: +60 3 55443870.
E-mail address: mhmamat@salam.uitm.edu.my (M.H. Mamat).

http://dx.doi.org/10.1016/j.ceramint.2015.11.083
0272-8842/

based techniques, such as MOCVD and PLD. Furthermore, due to the stability of the sputtering process, the growth of films can be well controlled and is reproducible [18].

The performance of UV photoconductive sensors based on ZnO film can be improved via several methods. For example, surface treatments (i.e., plasma and heat treatments) have been shown to increase the UV-sensing capability of ZnO film by improving the surface conditions, which allow for more efficient interactions with the surrounding environment [19–21]. In addition, coating the film with certain materials also results in an improved photoresponse of the UV-sensing device [22,23]. Furthermore, the surface area of the sensing material has been increased through the utilisation of 1D nanostructured with a small diameter and a dense array in the UV sensor, resulting in a UV sensor with improved performance [24]. Among these strategies for improving UV sensing, the preparation of small-diameter and dense 1D nanostructured arrays is the most fundamental aspect in the production of high-performance UV sensors. The preparation of a small-diameter and dense 1D nanostructured array via surface treatments and coating processes may further improve the performance of UV sensors and represents an approach that is challenging but nonetheless attractive, particularly if high quality ZnO 1D nanostructured arrays can be produced using a sputtering technique. Although grain boundary that exists in sputtered ZnO 1D nanostructured arrays is generally regarded to be worse for devices, the enhancement of surface area due to grain boundary can effectively improves the UV sensor performance. Therefore, the UV photoconductive sensor fabricated using sputtered ZnO nanocolumn arrays is expected to give higher performance than that of thin film-based UV sensor. Various sputtering parameters, including radio frequency (RF) power, deposition pressure, and the insertion of oxygen, may influence the deposition process and the quality of the resulting ZnO film. Sputtered ZnO films produced with oxygen introduced during the deposition have shown different optical, structural, and electrical characteristics when prepared under different oxygen flow rates [25–27]. Therefore, variations in the oxygen flow rate are expected to result in sputtered-ZnO-based UV photoconductive sensors with different performance characteristics. Generally, the growth of ZnO 1D nanostructured arrays is most likely determined by surface energy. According to Shet et al., substrate temperature played important role to the growth of nanostructured arrays [28]. Insertion of oxygen gas during sputtering process is also essential for 1D nanostructured growth. According to Chou et al., higher oxygen content or oxygen partial pressure during sputtering process results in higher area density of 1D ZnO nanostructures [29]. They explained that at higher oxygen partial pressure, there will be more collision between the oxygen and substrate, creating more energetic or active sites on the substrate in the process, which enhance the growth of the ZnO nanostructures. Besides, the addition of oxygen also enhances the (002) orientation or the *c*-axis preferred growth and forms single crystalline ZnO.

Herein, we report the fabrication of UV photoconductive sensors using highly transparent, dense, and small-diameter ZnO 1D nanostructured in form of nanocolumn arrays, which were prepared via catalyst-free RF magnetron sputtering at different oxygen flow rates. In addition, the prepared ZnO nanocolumn arrays have thicknesses of less than 100 nm, which is rare among ZnO films used in highly responsive UV photoconductive sensors. These fabricated sensors exhibit high sensitivity on the order of 10^4, which indicates that sputtered ZnO nanocolumn arrays are a promising sensing material for UV photoconductive sensors. Our study also reveals that the performance of the UV photoconductive sensors differs when the sensors are fabricated with ZnO nanocolumn arrays prepared at different oxygen flow rates.

2. Experimental procedure

ZnO nanocolumn arrays were deposited on a glass substrate without a catalyst using an RF magnetron sputtering (SNTEK, Korea) technique at a low power of 50 W. The nanocolumn arrays were deposited using a pure ZnO target (4 in., Process Materials, USA, 99.99%) at a deposition pressure of 0.67 Pa and a substrate temperature of 100 °C for 30 min. After a base pressure of 1×10^{-4} Pa was achieved in the chamber, pure argon and oxygen gases were fed into the chamber for the deposition process. During this process, the flow rate of argon was fixed at 45 sccm, whereas the flow rate of oxygen was varied from 0 to 25 sccm. The sample was subsequently removed from the deposition chamber and annealed in air for 1 h at 500 °C. To complete the metal–semiconductor–metal (MSM)-type ultraviolet photoconductive sensor structure, 60-nm-thick Al-metal contacts were deposited onto the samples with inter-electrode distances of 2 mm using a thermal evaporator at a deposition pressure of 4×10^{-4} Pa. A schematic diagram of sputtered ZnO nanocolumn array-based UV photoconductive sensor is shown in Fig. 1.

The surface morphology and cross-sections of the ZnO nanocolumn arrays were characterised by field-emission scanning electron microscopy (FESEM, JEOL JSM-7600F). The crystallinity of the samples was characterised using X-ray diffraction (XRD, Panalytical X'pert Pro). The optical properties of the nanocolumn arrays were characterised using ultraviolet–visible–near-infrared (UV–vis–NIR) spectrophotometry (Perkin Elmer Lambda 750). The current–voltage (*I*–*V*) characteristics of the samples were investigated using a two-probe *I*–*V* measurement system (Keithley 2400). UV photoresponse measurements of the fabricated sensors were

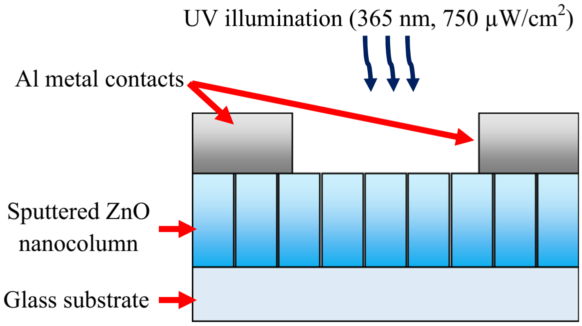

Fig. 1. A schematic diagram of sputtered ZnO nanocolumn array-based UV photoconductive sensor.

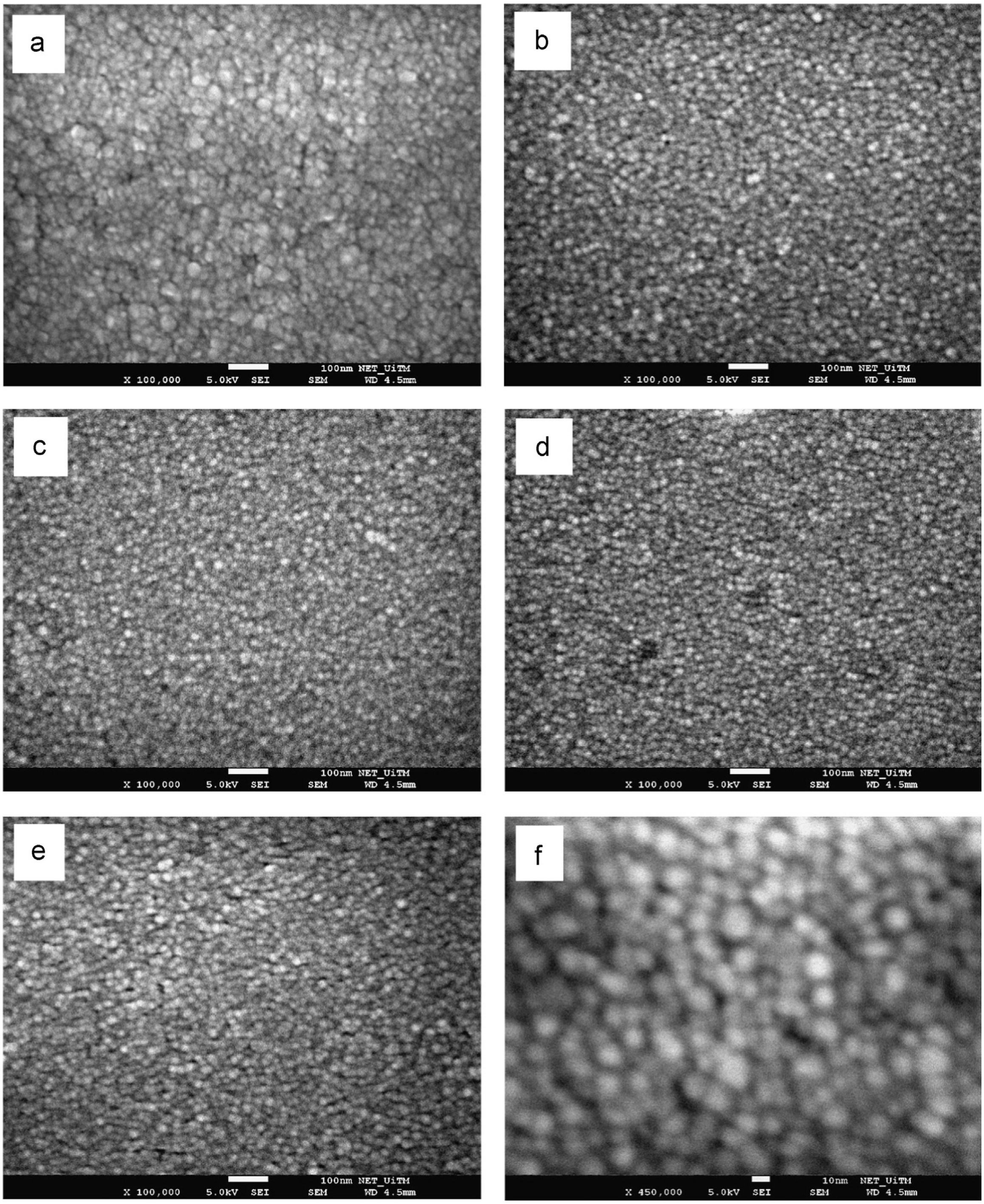

Fig. 2. Surface morphology of sputtered ZnO nanocolumn arrays prepared at oxygen flow rates of (a) 0, (b) 5, (c) 10, (d) 15, and (e) 25 sccm. (f) Magnified FESEM image of sputtered ZnO nanocolumn arrays prepared at an oxygen flow rate of 10 sccm.

performed using a UV photocurrent measurement system (Keithley 2400) operated at 365 nm with a power density of 750 μW/cm2 and a bias voltage of 10 V.

3. Results and discussion

The FESEM images of the sputtered ZnO nanocolumn arrays on glass substrates prepared at oxygen flow rates ranging from 0 to 25 sccm are shown in Fig. 2(a)–(f). These images indicate that the nanocolumns were densely deposited on the glass substrate using catalyst-free RF magnetron sputtering. The FESEM image of a sample prepared without oxygen (0 sccm) shows that the uniformity of the sample is poor because the film consists of both large- and small-diameter nanocolumns. However, when oxygen was flowed during the sputtering process, films with high uniformity were deposited; these films consist of well-distributed, small-diameter ZnO nanocolumn arrays on the substrate, as shown

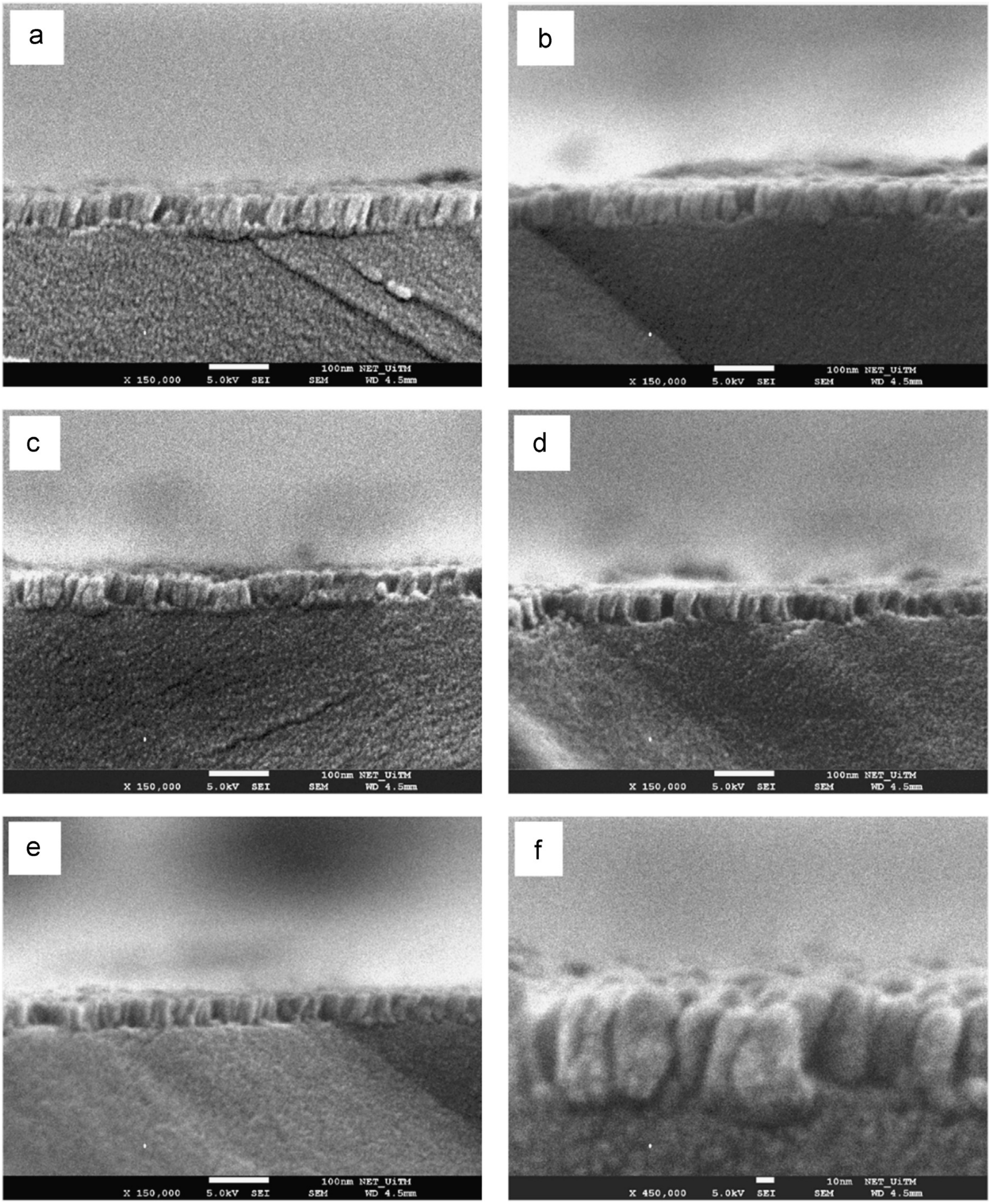

Fig. 3. Cross-sectional images of sputtered ZnO nanocolumn arrays prepared at oxygen flow rates of (a) 0, (b) 5, (c) 10, (d) 15, and (e) 25 sccm. (f) 450,000 × magnified cross-sectional image of sputtered ZnO nanocolumn arrays prepared at an oxygen flow rate of 10 sccm.

in Fig. 2(b)–(e). The 450,000 × magnified FESEM image of ZnO nanocolumn arrays prepared at 10 sccm shown in Fig. 2 (f) reveals that the nanocolumns have a small diameter of 10 to 20 nm and are uniformly deposited on the substrate. The average diameter of the nanocolumns was estimated from the FESEM images as 24, 19, 17, 15, and 14 nm when prepared at oxygen flow rates of 0, 5, 10, 15, and 25 sccm, respectively. These results indicate that the diameter of the sputtered nanocolumns decreased incrementally as the nanocolumns were grown at higher oxygen flow rates.

The cross-sectional images of sputtered ZnO nanocolumn arrays prepared at oxygen flow rates of 0, 5, 10, 15, and 25 sccm are shown in Fig. 3(a)–(e). The images reveal that the ZnO films deposited by RF magnetron sputtering contained highly dense, thin, and aligned ZnO nanocolumn arrays. The magnified image in Fig. 3(f) of a sputtered ZnO film prepared at an oxygen flow rate of 10 sccm shows that the nanoscopic aligned ZnO nanocolumn arrays were vertically deposited on the glass substrate. The thickness of these films were estimated from the FESEM images to be 80, 70, 67, 58, and 53 nm for films prepared at oxygen flow rates of 0, 5, 10, 15, and 25 sccm, respectively.

The slight decrease in both the thickness and the nanocolumn diameter of the nanocolumn arrays with increasing oxygen flow rates is due to the increase of electronegative oxygen in the sputtering discharge [30]. This electronegative oxygen, which is highly affinitive to electrons in the discharge, reduces the plasma density and thus, results in fewer positive argon ions. This condition reduces the sputtering rate and finally, reduces both thickness and diameter of the nanocolumns when more oxygen is introduced into the sputtering chamber. The decrease in both the thickness and the diameter of the nanocolumn arrays with increasing oxygen flow rates may also be caused by differences in the sputtering yield of the two gases (argon and oxygen) [31]. The rare-gas ions of argon have a higher sputtering rate compared to the reactive-gas ions of oxygen. In addition, high oxygen flow rates also decreased the argon partial pressure and, therefore, decreased the number of bombarding argon ions, which decreased the deposition rate of ZnO [26]. A high flow rate of oxygen may also disturb the bombardment of argon ions towards the ZnO target because oxygen molecules may adsorb onto the target surface [32].

The XRD patterns of the sputtered ZnO nanocolumn arrays prepared at oxygen flow rates of 0 and 10 sccm are shown in Fig. 4. The diffraction patterns of the nanocolumn arrays exhibit peaks that can be indexed to the ZnO hexagonal phase with a wurtzite structure (Joint Committee on Powder Diffraction Standards (JCPDS) PDF no. 36-1451). The broad peak located between 20° and 40° is due to the glass substrate [33]. The XRD patterns of sputtered nanocolumn arrays prepared at an oxygen flow rate of 0 sccm exhibit three peaks corresponding to the (100), (002), and (101) planes of ZnO. However, the XRD spectrum of the sample prepared at an oxygen flow rate of 10 sccm shows only the (002) peak, which indicates that the nanocolumns preferentially grow along the *c*-axis or perpendicular to the substrate. In addition, the prominent (002) peak in the spectrum of the nanocolumn arrays prepared at an oxygen flow rate of 10 sccm is more intense than that in the spectrum of the nanocolumn array prepared at an oxygen flow rate of 0 sccm (without oxygen). This result indicates that the crystallinity of the prepared nanocolumn arrays improved when oxygen was introduced during the deposition process. Because of the high-energy bombardment of argon ions on the target with a high sputtering rate in the absence of oxygen, structural defects, such as dislocations, are most likely formed, which diminish the crystallinity of the films [31]. Therefore, the introduction of oxygen is essential during the sputtering process to improve the crystallinity of the ZnO film. A similar observation has also been reported by Wang et al., who studied RF magnetron sputtered ZnO films at oxygen flow rates between 0 and 10 sccm [33]. According to their results, the diffraction pattern of a ZnO film grown without oxygen contained numerous diffraction peaks corresponding to the (002), (101), (102), (103), (201), and (004) planes. However, when oxygen was introduced during the sputtering process, the film grew preferentially along the *c*-axis or (002) plane, and the other diffraction peaks disappeared, except the (002) and (004) peaks. According to their results, this (002)-plane preferential growth became more pronounced with higher oxygen flow rates. It was suggested that this increased (002) preferential growth with increasing oxygen flow rates was due to a decrease in the concentration of oxygen vacancies.

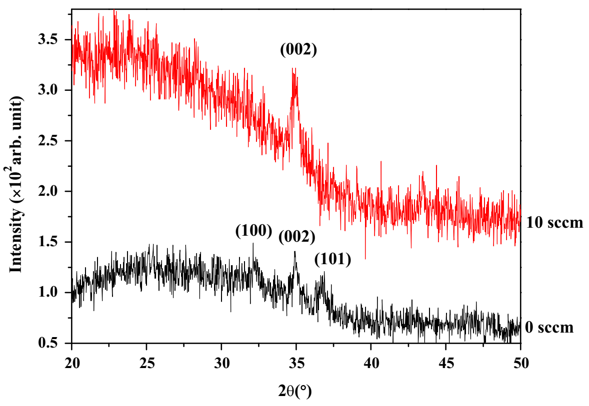

Fig. 4. XRD patterns of sputtered ZnO nanocolumn arrays prepared at oxygen flow rates of 0 (i.e., in the absence of oxygen) and 10 sccm.

Fig. 5(a) shows the transmittance spectra of the sputtered ZnO nanocolumn arrays prepared with different flow rates of oxygen in the wavelength range from 300 to 1500 nm. These spectra demonstrate that the nanorod arrays exhibit good optical transmittance in the visible (400–800 nm) and near-infrared (800–1500 nm) ranges. The spectra also reveal that with the introduction of oxygen, the transmittance of the nanocolumn arrays improves relative to that of a film prepared in the absence of oxygen. The average transmittance in the visible region of ZnO nanocoumn arrays prepared with oxygen flow rates of 5, 10, 15, and 25 sccm was estimated to be 96%, 98%, 97%, and 97%, respectively. Notably, the average transmittance in the visible region of the ZnO nanocolumn arrays prepared in the absence of oxygen (0 sccm) was approximately 90%. These results demonstrate that the sputtering process produces ZnO nanocolumn arrays with transparencies in the visible region greater than 90%. The lower transmittance of the ZnO nanocolumn arrays prepared without oxygen may be due to poor uniformity of the film, as shown in the FESEM image in Fig. 2(a). According to Ahn et al., the deposition of a ZnO film without oxygen in a sputtering process produced a film with a rough surface that exhibited degraded optical transmittance [31]. Fig. 5(b) shows the absorbance spectra of ZnO nanocolumn arrays prepared using different oxygen flow rates. The absorbance spectra reveal that all of the samples exhibit good UV absorption properties at wavelengths of less than 400 nm, with an absorption peak centred at approximately 365 nm. The strong absorption properties in the UV region indicate that the sputtered nanocolumn arrays are suitable for UV photoconductive sensor applications.

The optical bandgap energy of sputtered ZnO nanocolumn arrays, in the high absorption region could be expressed by the

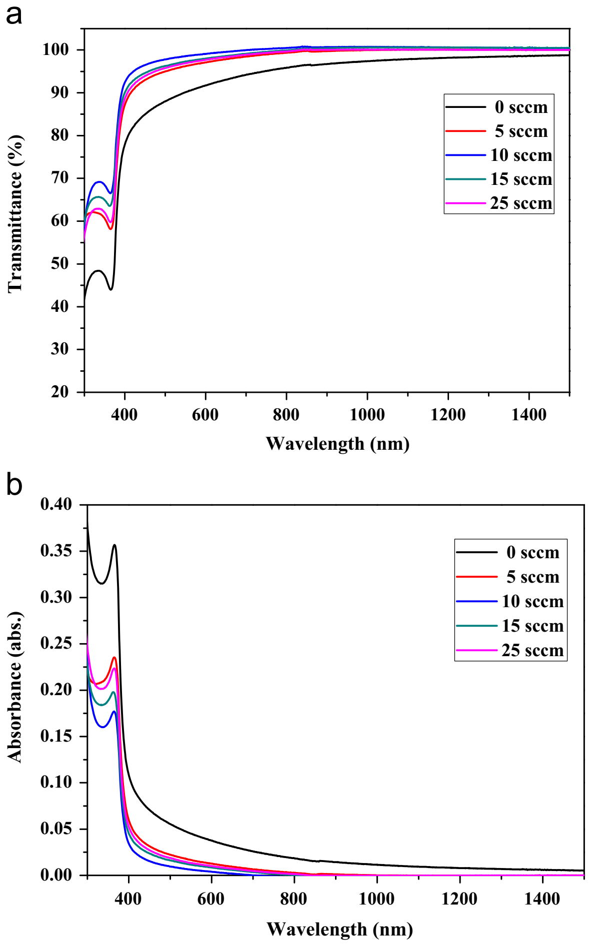

Fig. 5. UV–vis–NIR (a) transmittance and (b) absorbance spectra of sputtered ZnO nanocolumn arrays prepared at different oxygen flow rates.

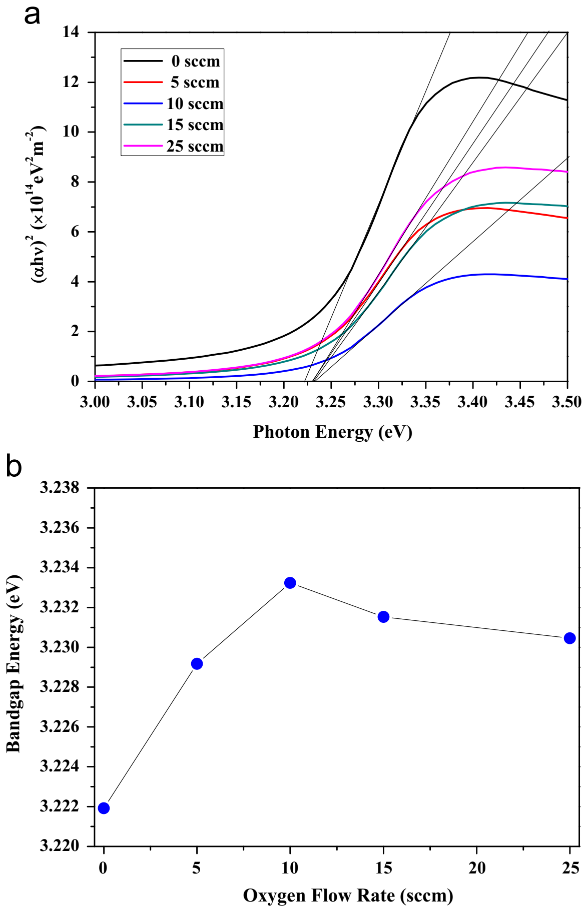

Fig. 6. (a) Estimation of the optical bandgap energy, Eg, of ZnO nanocolumn arrays using Tauc's plot as a function of oxygen flow rate. (b) Plot of optical bandgap versus oxygen flow rate.

following Tauc's relation (1) [34]:

$$\alpha h\nu = B\left(h\nu - E_g\right)^n \tag{1}$$

where $h\nu$ is the photon energy, E_g is the optical band gap and B is an energy-independent constant having values between 1×10^5 and $1\times10^6\ \mathrm{cm}^{-1}\ \mathrm{eV}^{-1}$, which is depending on electron–hole mobility [35]. The α is an absorption coefficient, which can be calculated using transmittance data that has been estimated from Lambert`s law as shown in the following Eq. (2):

$$\alpha = \frac{1}{t}\ln\left(\frac{1}{T}\right) \tag{2}$$

where t is the thickness and T is the transmittance of the of sputtered ZnO nanocolumn arrays. The n represents an exponent which can be a different values depending on the nature of the electronic transitions responsible for the optical absorption; $n = 1/2$ and 3/2 for direct allowed and forbidden direct transitions, respectively, $n = 2$ and 3 for indirect allowed and forbidden indirect transition, respectively. Due to the fact that ZnO is a direct band gap material, the value of n is taken as 1/2 and the optical band gap is determined from the Tauc's plot as shown in Fig. 6(a). The band gap was estimated as the energy at which the extrapolated linear part of $(\alpha h\nu)^2$ versus $h\nu$ plot intersects the photon energy (x-axis). The optical band gap energy estimation of the sputtered ZnO nanocolumn arrays with respect to oxygen flow rate is shown in Fig. 6(b). The band gap energy of ZnO nanocolumn arrays prepared with oxygen flow rates of 0, 5, 10, 15, and 25 sccm was estimated to be 3.222, 3.229, 3.233, 3.231, and 3.230 eV, respectively. According to Ansari et al., the band gap energy of ZnO may be influenced by the oxygen vacancies in the ZnO lattice and lattice disorder represented by band tail or Urbach energy [36]. The authors explained that the oxygen vacancies in the ZnO lattice decrease band gap energy, which was also in agreement with the other reported works [37,38]. Moreover, the lattice disorder can generate a band tail below the conduction band, which also reduces band gap energy [39–41]. The oxygen vacancies and lattice disorder are common defects in the sample prepared without or under low oxygen ambient in the sputtering process [42–45]. Therefore, the ZnO nanocolumn arrays prepared without oxygen may have higher density of oxygen vacancies and lattice disorder as the sputtering process was conducted without oxygen. However, these defects were reduced when oxygen was introduced in the sputtering chamber up to 10 sccm. This condition subsequently increased the band gap energy of ZnO nanocolumn arrays when the oxygen flow rate was increased from 0 sccm to 10 sccm. The increase in band gap energy with the increased flow rate from 0 sccm to 10 sccm may also be related to the decrease in resistance value, as discussed in the *I–V* plot, because the ZnO band gap is sensitive to small changes in carrier concentration, grain boundary configuration, and film stress [46]. However, the band gap energy decreased when the oxygen flow rate was further increased to 25 sccm. Under rich oxygen ambient in the sputtering process, oxygen interstitials have low formation energies, which can occupy the interstitial sites of the ZnO lattice [47]. Furthermore, excessive oxygen may produce structural defects that contribute to lattice disorder and poor crystallinity [48,49]. This condition introduces states in the lower part of the band gap, and these states can accept two electrons, thereby acting as compensation centres [47]. This energy state may reduce the electron concentrations, which causes the shift in the Fermi level to lower energies and increases the Urbach energy or band tailing, thereby decreasing the band gap energy of ZnO nanocolumn arrays at higher oxygen flow rates greater than 10 sccm. This energy state may be the reason behind the increased resistance when the ZnO nanocolumn arrays were prepared at an oxygen flow rate greater than 10 sccm, as discussed in the *I–V* plot.

The structural disorder in the sputtered ZnO nanocolumn arrays was characterised by the slope of the Urbach tail or Urbach energy. The Urbach energy can be used to evaluate the defective concentration in the sputtered ZnO nanocolumn arrays. The Urbach law states that α near the band edges is exponentially dependent on photon energy, $h\nu$, as shown by the following equation (3)[50]:

$$\alpha = \alpha_0 \exp\left(\frac{h\nu}{E_u}\right) \tag{3}$$

where E_u is the Urbach energy, and α_0 is a constant. Thus, the Urbach energy can be determined through the plot of ln (α) versus photon energy, in which the value of the Urbach energy is equal to the reciprocal gradient of the linear potion of the plot. The Urbach plots of the nanocolumn arrays are shown in Fig. 7(a).

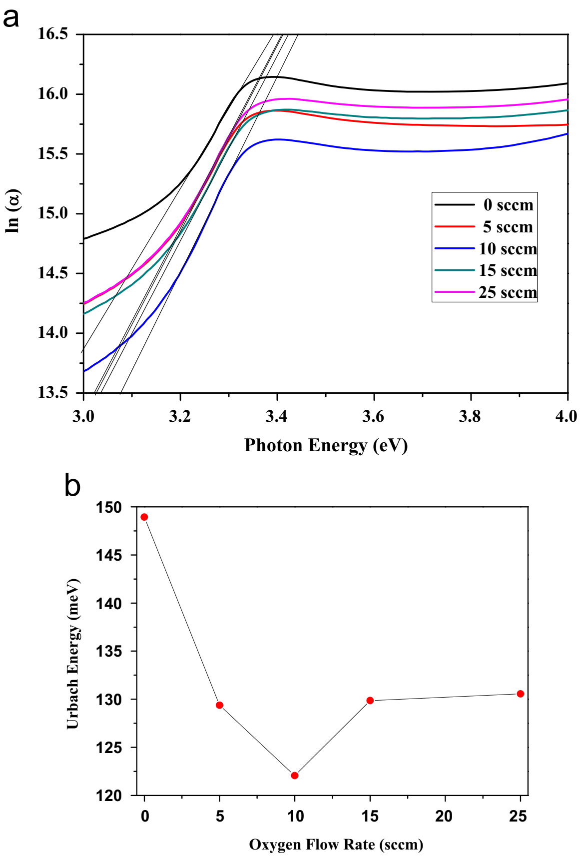

Fig. 7. (a) Plot of ln(α) versus photon energy for ZnO nanocolumn arrays prepared at various oxygen flow rates. (b) Urbach energy E_u of ZnO nanocolumn arrays as a function of oxygen flow rates.

The Urbach energy has the dimension of energy related to the width of the localised states in the band gap. This energy is considered a free parameter indicating the effect of all possible defects. These defects may be originated during the film growth process, causing lattice disorders and generating stress in the film. The defects in ZnO lead to local electric fields that influence the band tails [51]. The plot in Fig. 7(b) reveals that the Urbach energy reduced when the oxygen flow rate was increased from 0 sccm to 10 sccm but increased when the flow rate was increased to 25 sccm. The calculated Urbach energy values of sputtered ZnO nanocolumn arrays prepared at oxygen flow rates of 0, 5, 10, 15, and 25 sccm were 149, 129, 122, 130, and 131 meV, respectively. The Urbach energy values inversely varied with the optical band gap energy. During the formation of ZnO nanocolumn arrays at different oxygen flow rates, some defects were formed that produced localised states in the films. Thus, the increase in the width of the localised states, which was represented by the Urbach energy, decreased the optical band gap energy. This result suggested that the structural defects were reduced when oxygen was introduced up to 10 sccm but increased when the flow rate was increased to 25 sccm. At the flow rate of 0 sccm, the corresponding Urbach energy was high at 149 meV and decreased very slowly with the increase in flow rate up to 10 sccm. As the flow rate increased to 10 sccm, the oxygen atoms diffused, occupied the correct site in the ZnO crystal lattice, grew at lower surface energy, and finally improved the structural properties of the nanocolumn arrays. The decrease in Urbach energy was also related to the reduction in oxygen vacancy defects. The density of oxygen vacancy defects in the sputtered ZnO nanocolumn arrays was expected to reduce when the oxygen flow rates increased up to 10 sccm, which may decrease the density of mid-gap states induced by oxygen vacancies [52]. As a result of the reduction in sub-gap states below the conduction bands, the optical band gap energy of the ZnO nanocolumn increased at the oxygen flow rate of up to 10 sccm. According to Seo et al., the reduced band gap of nonstoichiometric oxide semiconductor films was caused by the sub-oxide states associated with the oxygen vacancies [53]. However, Urbach energy increased at the flow rates of more than 10 sccm, suggesting the irregular atomic arrangement of ZnO nanocolumn arrays at higher oxygen flow rates. When the oxygen content was too high with high flow rates, the atomic arrangement in the lattice structure became disordered and the oxygen atoms randomly occupied the interstitial sites, thereby degrading the crystal quality of ZnO nanocolumn arrays. Bachari et al. reported that low oxygen content in the film structure causes an increase in crystallographic defects, whereas high oxygen content destroys the stoichiometry because of the lower surface mobility of the deposited atoms and lower kinetic energy for surface diffusion [49]. In addition, adding more oxygen into the discharge may produce more neutral oxygen atoms, which diffuse into films without sufficient energy, thereby creating additional unexpected defects [45,54]. Excessive oxygen in low-power sputtering causes a decrease in the surface mobility of the deposited atoms and provides less energy for surface diffusion. Consequently, the crystallinity of the deposited films decreases. [48,49].

The *I–V* characteristics of the sputtered ZnO nanocolumn arrays prepared at different oxygen flow rates are shown in Fig. 8. The linear *I–V* curves indicate that the sputtered ZnO nanocolumn arrays form a good ohmic contact with the Al metal. The result also shows that the current, with respect to the supplied voltage, increased for the sputtered ZnO nanocolumn arrays prepared at oxygen flow rates as high as 10 sccm. However, the current decreased when the flow rate of oxygen was further increased to 25 sccm. The resistance of the sputtered ZnO nanocolumn arrays prepared at oxygen flow rates of 0, 5, 10, 15, and 25 sccm was 16.7, 5.2, 2.3, 9.8, and 16.5 GΩ, respectively.

Based on several studies, the introduction of oxygen during the sputtering process normally reduces the carrier concentration because the occurrence of native donors, such as zinc interstitials and oxygen vacancies, is reduced [26,32]. However, the polycrystalline nature, structural defects, and poor uniformity of the sample without oxygen might be the factors that increase the resistance of the film. In our study, the introduction of oxygen at flow rates of up to 10 sccm improved the electronic conduction in the film, as shown by the decreased resistance. The addition of oxygen is believed to result in films with good electron mobility that is facilitated by the improved uniformity, low structural disorder (Urbach energy), and crystallinity of the film compared to that of the sample deposited in the absence of oxygen, as shown in the FESEM micrographs (Fig. 2), Urbach energy plot (Fig. 7) and XRD patterns (Fig. 4). The nanocolumn arrays prepared in the absence of oxygen may contain numerous dislocations and structural defects, which result in electron scattering and, thus, high resistance in the film. This defects may also traps electron with long lifetime, which reduce the carrier concentration in the films. When oxygen was introduced during the sputtering process, the occurrence of structural defects was reduced, which improved the conductivity of the films. However, the excessive oxygen introduced at flow rates greater than 10 sccm during the sputtering process produced films with high resistance because the oxygen ions most likely situate at the interstitial position of the lattice, thereby forming oxygen interstitials and/or antisite defects [55]. These acceptor-like defects consume electrons in the film to increase the resistance of the film. Furthermore, high numbers of oxygen molecules facilitated by a high oxygen flow rate during the sputtering process may be chemisorbed onto the nanocolumn arrays and may increase the band bending, which decreases the electron mobility of the film [26]. This result also consistent with the calculated Urbach energy as discussed above. Similar observations have been reported by Kim et al., who studied the effect of the oxygen/argon flow-rate ratio on the growth of Ga-doped ZnO films [27]. According to their analysis, an increase in the oxygen/argon flow-rate ratio up to certain value (i.e., 0.25) resulted in reduced resistivity of the film due to enhanced crystallinity and increased mobility; however, at high oxygen/argon flow-rate ratios (i.e., greater than 0.25), the resistivity increased due to the segregation of oxygen atoms in the lattice.

The spectra from the photocurrent measurements for the sputtered ZnO nanocolumn arrays deposited at different oxygen flow rates are shown in Fig. 9(a). The results indicate that the photocurrent of the sensors increased for the sputtered nanocolumn arrays prepared at oxygen flow rates of up to 10 sccm. However, the photocurrent of the sensor decreased for the nanocolumn arrays prepared at oxygen flow rates of 15 and 25 sccm. The photocurrents (dark current) of the sensors were 1.88×10^{-7} (1.28×10^{-11}), 2.82×10^{-7} (1.54×10^{-11}), 4.35×10^{-7} (1.98×10^{-11}), 3.51×10^{-7} (1.92×10^{-11}), and 1.38×10^{-7} (1.13×10^{-11}) A for the sputtered nanocolumn arrays prepared at oxygen flow rates of 0, 5, 10, 15, and 25 sccm, respectively. The improvement in the photocurrent value of sputtered ZnO nanocolumn arrays prepared at oxygen flow rates up to 10 sccm may be due to a decrease in the resistance of the nanocolumn arrays, as shown in the I–V measurement data. This photocurrent improvement may also be attributed to the improved structural properties of the sputtered ZnO nanocolumn arrays prepared at an oxygen flow rate of 10 sccm, which resulted in an enhanced mobility of the photoexcited electron across the Al contacts. However, at oxygen flow rates greater than 10 sccm, the oxygen ions may occupy the interstitial positions of the lattice sites to form oxygen interstitials or/and antisite defects that may again inhibit electronic conduction in the ZnO films [55]. As a result, the photocurrent and the dark current of the sensors decreased when sputtered ZnO nanocolumn arrays prepared at oxygen flow rates of 15 and 25 sccm were used. The resistance values of these

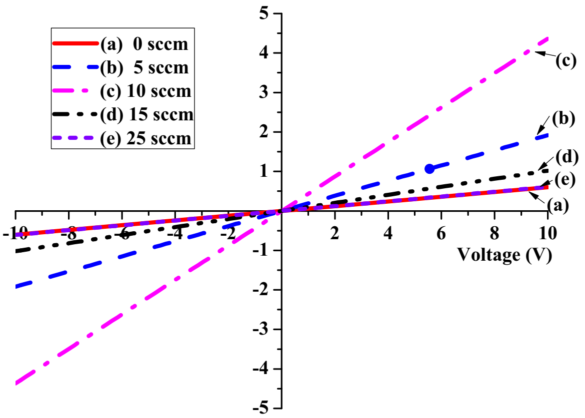

Fig. 8. Current–voltage (*I–V*) plots of the sputtered ZnO nanocolumn arrays prepared at different oxygen flow rates.

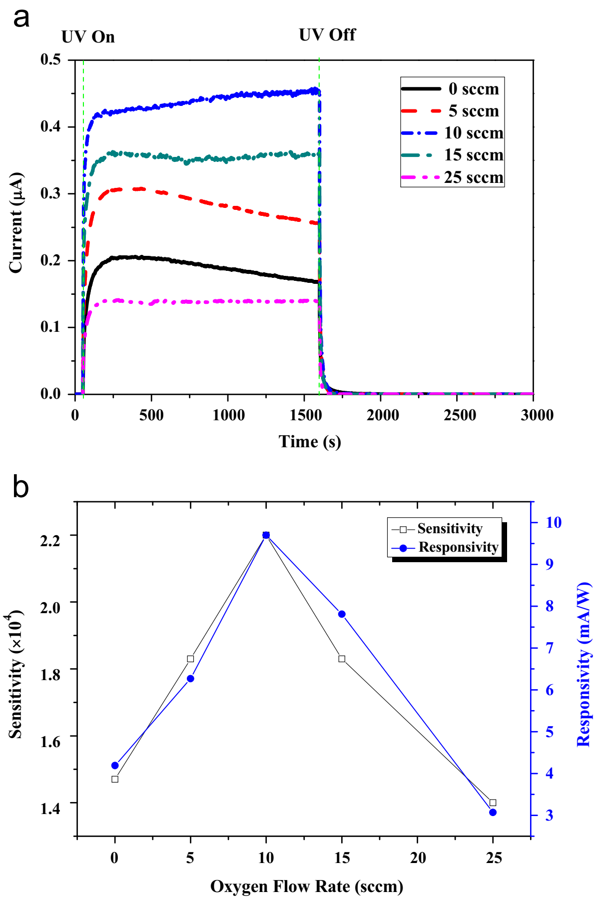

Fig. 9. (a) Photoresponse spectra of the UV photoconductive sensors using sputtered ZnO nanocolumn arrays prepared at different oxygen flow rates; the spectra were measured under UV illumination (365 nm, 750 µW/cm^2) and a 10-V bias. (b) The variations in sensitivity and responsivity of the UV photoconductive sensors using sputtered ZnO nanocolumn arrays prepared at different oxygen flow rates.

samples were also greater than that of the nanocolumn arrays prepared at an oxygen flow rate of 10 sccm, as revealed by the *I–V* curves. These oxygen defects also induce the formation of a non-conductive barrier or a depletion region and, thus, upward band bending [56]. From these photocurrent measurement results, the responsivity of the devices was calculated using the following equation (4) [57]:

$$R = \frac{I_{ph} - I_{dark}}{P_{op}} \tag{4}$$

where I_{ph} is the photocurrent, I_{dark} is the dark current, and P_{op} is the optical power of the UV source (4.49×10^{-5} W). The results of these calculations indicate that the sputtered ZnO nanocolumn arrays prepared at an oxygen flow rate of 10 sccm exhibited the highest responsivity, with a value of 9.70 mA/W. The responsivities of the other sensors were 4.19, 6.27, 7.81, and 3.07 mA/W for the sputtered nanocolumn arrays prepared at oxygen flow rates of 0, 5, 15, and 25 sccm, respectively.

Interestingly, the sensitivity of the sensors, which is defined as the photocurrent-to-dark-current ratio, was very high: on the order of 10^4 for all of the ZnO nanocolumn array sensors. This high sensitivity of the sputtered ZnO nanocolumn array-based UV photoconductive sensors is attributed to the large surface area facilitated by the high density and small diameter of the nanocolumns [24]. The sensitivity of the sensors was 1.47×10^4, 1.83×10^4, 2.20×10^4, 1.83×10^4, and 1.40×10^4 for sputtered nanocolumn arrays prepared at oxygen flow rates of 0, 5, 10, 15, and 25 sccm, respectively. This result indicates that the sensitivity of sputtered ZnO nanocolumn array-based UV photoconductive sensors can be enhanced through an increase in the oxygen flow rate to 10 sccm during the sputtering process. The variations in sensitivity and responsivity of the UV photoconductive sensors using sputtered ZnO nanocolumn arrays prepared at different oxygen flow rates are depicted in Fig. 9(b).

Based on several reports, the sensitivity of the sensor is generally influenced by the surface area availability and the surface conditions of the nanocolumns that are capable of promptly adsorbing and desorbing oxygen [24,58,59]. The oxygen adsorption and desorption processes can be explained as follows. In the dark, oxygen molecules tend to adsorb onto nanocolumn surfaces by capturing free electrons and producing adsorbed oxygen ions, as shown by the following equation (5) [60,61]:

$$O_2 + e^- \rightarrow O_2^-, \tag{5}$$

where O_2 is an oxygen molecule, e^- is a free electron, and O_2^- is an adsorbed oxygen ion on the nanocolumn surface. The adsorbed oxygen ions create a barrier near the surface that generates a low current prior to UV illumination. When the nanocolumns are irradiated with UV light, photogenerated electron–hole pairs are produced at the surface according to the following Eq. (6):

$$h\nu \rightarrow h^+ + e^-, \tag{6}$$

where $h\nu$ is the photon energy of the UV light, h^+ is the photogenerated hole in the valence band, and e^- is the photogenerated electron in the conduction band. The photogenerated holes recombine with the adsorbed oxygen ions on the surface, thereby producing oxygen molecules; this reaction also eliminates the barrier near the nanocolumn surface. This process is described by following Eq. (7):

$$O_2^- + h^+ \rightarrow O_{2.} \tag{7}$$

Simultaneously, the desorption of oxygen ions adsorbed onto the nanocolumn surface produces photogenerated electrons in the conduction band, which increases the film conductivity and contributes to the photocurrent. When the UV light is switched off, the oxygen once again starts to adsorb onto the nanocolumn surface, which decreases the conductivity of the sensor. From our results, the high density and small diameter of the sputtered nanocolumn arrays facilitate a large surface area for oxygen adsorption and desorption processes, which results in the high sensitivity of the devices [24]. In addition, high UV sensitivity of the ZnO nanocolumn arrays resulted from the increase in photocurrent magnitude [62]. This finding was expected from the electrical resistance data, which showed an inverse relation between the photocurrent and sensitivity with the electrical resistance of the samples, similar to previously reported work [63]. According to the resistance data, the resistance of the ZnO nanocolumn arrays reduced when the oxygen flow rate increased from 0 sccm to 10 sccm but increased when the flow rate increased to 25 sccm. By contrast, the photocurrent and sensitivity of the ZnO nanocolumn array-based UV photoconductive sensor increased when the flow rate increased from 0 sccm to 10 sccm but decreased when the flow rate increased to 25 sccm. The high photocurrent obtained for ZnO nanocolumn arrays prepared at 10 sccm may be attributed to its enhanced crystallinity and low Urbach energy, which indicated that the structural disorder of the sample was the lowest. Given this condition, the ZnO nanocolumn arrays prepared at 10 sccm had more photogenerated free electrons, which could be accredited to the significantly suppressed recombination of photogenerated charge carriers [46,64]. This result suggested that the photocurrent of the sensor increased when the resistance and structural disorder of the sample decreased, contributing to high sensitivity of the samples, particularly for the ZnO nanocolumn arrays prepared at the oxygen flow rate of 10 sccm.

The relationship of the sensor behaviour to the adsorption and desorption of oxygen was studied by Jun et al [57]. They measured fabricated UV sensors under different atmospheric pressures (0.1–1.0 atm) with different oxygen levels. They found that the photoresponse decay time constant of the sensor increased with decreasing atmospheric pressure. Because the lower atmospheric pressure caused a lower oxygen content, the ability of the sensor to return to its initial state (dark current) was reduced as the adsorption of oxygen onto the ZnO surface was reduced. This condition increased the decay time constant of the device as the atmospheric pressure was lowered. Similarly, Cheng et al. also demonstrated the dependency of ZnO on the oxygen adsorption process [65]. They fabricated ZnO microtube ultraviolet photodetectors using a microwave-heating growth method. They analysed their fabricated sensors in different environments (e.g., air, O_2, Ar, and N_2) and found that the sensor responses and the photocurrent were highly dependent on the environment. It was found that the response of the sensor was fastest in the oxygen ambient environment, with rise and decay times of 2.9 and 100 s, respectively. They acknowledged that this sensing behaviour was due to the rapid desorption and adsorption of oxygen on the nanorod surface as the UV illumination was being turned on and off in the rich oxygen environment. Ok et al. fabricated a ZnO nanowire-carbon nanotube (CNT) heterostructure-based UV photoconductive sensor using the CVD technique [66]. By using Au for the metal contacts, the fabricated sensor demonstrated a high response with a photocurrent of approximately 33 μA under 365-nm UV light with an optical power density of 74 mW/cm^2. They also reported that their fabricated sensors did not work under vacuum, which indicated that the response of their sensors was governed by the oxygen adsorption and desorption process.

We also observed that photocarrier relaxation or photocurrent decay under UV illumination occurred for the sputtered ZnO nanocolumn arrays prepared at oxygen flow rates of 0 and 5 sccm. However, for the sputtered ZnO nanocolumn arrays prepared at oxygen flow rates of 10 sccm or greater, this photocurrent decay was reduced. Photocurrent decay under UV illumination mainly occurs due to photoexcited electron trapping by the surface re-adsorbed oxygen molecules [22]. According to Bera et al., this condition is also due to the existence of structural defects, such as positively charged Zn interstitials, on the nanorods, which act as recombination centres for the photoexcited electrons [67]. Because the recombination centres have a longer lifetime, the re-excitation process of recombined electrons cannot occur as fast as the recombination process, which decreases the photocurrent value under steady UV illumination. This result indicates that the photocurrent decay under UV illumination could be reduced through the introduction of oxygen at a high flow rate during the sputtering process, which decreases the occurrence of defects (i.e., recombination centres for photoexcited electrons) in the nanocolumn arrays and thus reduces the photocurrent decay under steady UV illumination.

The rise (decay) time constants of the sensors were calculated from the photocurrent spectra using following Eqs. (8), and (9):

$$I = I_0\left[1 - \exp\left(-\frac{t}{\tau_r}\right)\right] \text{ : rise process with UV illumination on} \tag{8}$$

$$I = I_0 \exp\left(-\frac{t}{\tau_d}\right) \text{ : decay process with UV illumination off.} \tag{9}$$

Here, I is the magnitude of the current, I_0 is the saturated photocurrent, t is the time, τ_r is the rise time constant, and τ_d is

Table 1

Characteristics of UV photoconductive sensors based on sputtered ZnO nanocolumn prepared at different oxygen flow rates; the measurements were performed under 365-nm UV illumination with an optical power of 750 μW/cm^2 and a 10-V bias.

Oxygen flow rate (sccm)	Dark current (A)	Photocurrent (A)	Rise time constant (s)	Decay time constant (s)	Photocurrent-to-dark current ratio or Sensitivity	Responsivity (mA/W)
0	1.28×10^{-11}	1.88×10^{-7}	13	14	1.47×10^4	4.19
5	1.54×10^{-11}	2.82×10^{-7}	7	8	1.83×10^4	6.27
10	1.98×10^{-11}	4.35×10^{-7}	6	7	2.20×10^4	9.70
15	1.92×10^{-11}	3.51×10^{-7}	5	5	1.83×10^4	7.81
25	1.13×10^{-11}	1.38×10^{-7}	5	4	1.40×10^4	3.07

the decay time constant. The rise (decay) time constants of the sensors were estimated to be 13 (14), 7 (8), 6 (7), 5 (5), and 5 (4) s for the sputtered ZnO nanocolumn arrays prepared at oxygen flow rates of 0, 5, 10, 15, and 25 sccm, respectively. According to these calculation results, the rise and decay time constants of the sensors tended to decrease for the sputtered ZnO nanocolumn arrays prepared at higher oxygen flow rates. This result may be due to the higher surface-to-volume ratio of the sputtered ZnO nanocolumn arrays prepared at higher oxygen flow rates, which have smaller nanocolumn diameters [24,68]. In addition, this phenomenon may also be attributed to the shorter electron transmission lengths of the sputtered ZnO nanocolumn arrays prepared at higher oxygen flow rates compared to those of larger-diameter nanocolumn produced at low oxygen flow rates [69,70]. Thus, the sensors constructed with the arrays of small diameter and small thickness may exhibit low rise and decay time constants. The performances of the UV photoconductive sensors based on sputtered ZnO nanocolumn arrays prepared at different oxygen flow rates, which were measured under 365-nm UV light and a 10-V bias, are presented in Table 1.

4. Conclusions

UV photoconductive sensors were successfully fabricated using sputtered ZnO nanocolumn arrays prepared at different oxygen flow rates ranging from 0 to 25 sccm. The sputtered ZnO nanocolumn arrays had small diameters and thicknesses of less than 100 nm and were densely and uniformly deposited onto the glass substrate. The average diameter and thickness of the nanocolumn arrays were found to decrease as the oxygen flow rate increased. The resistance values of the sputtered ZnO nanocolumn arrays decreased when the arrays were prepared at higher oxygen flow rates up to 10 sccm; however, the resistance values decreased when the arrays were prepared at oxygen flow rates greater than 10 sccm. The photocurrent of the UV photoconductive sensors increased when sputtered ZnO nanocolumn arrays prepared at oxygen flow rate up to 10 sccm were used, but decreased for the sputtered ZnO nanocolumn arrays prepared at oxygen flow rates greater than 10 sccm. An extremely high sensitivity of the sensors (on the order of 10^4) was obtained when the sputtered ZnO nanocolumn arrays were used as the sensing element, with a maximum sensitivity of 2.20×10^4 for the sputtered ZnO nanocolumn arrays prepared at an oxygen flow rate of 10 sccm.

Acknowledgements

This work was supported by the Fundamental Research Grant Scheme (600-RMI/FRGS 5/3 (57/2015)), Research Acculturation Collaborative Effort (600-RMI/RACE 16/6/2 (9/2013)), and Long-Term Research Grant Scheme (600-RMI/LRGS 5/3 (3/2013)) from the Ministry of Higher Education of Malaysia. The authors also would like to thank the Research Management Institute (RMI) of UiTM and the Ministry of Higher Education of Malaysia for their financial support of this research.

References

[1] X. Gu, M. Zhang, F. Meng, X. Zhang, Y. Chen, S. Ruan, Influences of different interdigital spacing on the performance of UV photodetectors based on ZnO nanofibers, Appl. Surf. Sci. 307 (2014) 20–23.

[2] M.H. Mamat, Z. Khusaimi, M.Z. Musa, M.F. Malek, M. Rusop, Fabrication of ultraviolet photoconductive sensor using a novel aluminium-doped zinc oxide nanorod-nanoflake network thin film prepared via ultrasonic-assisted sol-gel and immersion methods, Sens. Actuators A: Phys. 171 (2011) 241–247.

[3] U.N. Maiti, K.K. Chattopadhyay, S. Karan, B. Mallik, Synthesis of a zinc oxide nanosheet–nanowire network complex by a low-temperature chemical route: Efficient UV detection and field emission property, Scr. Mater. 62 (2010) 305–308.

[4] W. Dai, X. Pan, C. Chen, S. Chen, W. Chen, H. Zhang, Z. Ye, Enhanced UV detection performance using a Cu-doped ZnO nanorod array film, RSC Adv. 4 (2014) 31969–31972.

[5] N.S. Ridhuan, K. Abdul Razak, Z. Lockman, A. Abdul Aziz, Structural and morphology of ZnO nanorods synthesized using ZnO seeded growth hydrothermal method and its properties as UV sensing, PLoS One 7 (2012) e50405.

[6] Y. Shen, X. Yan, Z. Bai, X. Zheng, Y. Sun, Y. Liu, P. Lin, X. Chen, Y. Zhang, A self-powered ultraviolet photodetector based on solution-processed p-NiO/n-ZnO nanorod array heterojunction, RSC Adv. 5 (2015) 5976–5981.

[7] M.H. Mamat, M.F. Malek, N.N. Hafizah, Z. Khusaimi, M.Z. Musa, M. Rusop, Fabrication of an ultraviolet photoconductive sensor using novel nanostructured, nanohole-enhanced, aligned aluminium-doped zinc oxide nanorod arrays at low immersion times, Sensors Actuators B: Chem. 195 (2014) 609–622.

[8] W. Lu, C. Jiang, D. Caudle, C. Tang, Q. Sun, J. Xu, J. Song, Controllable growth of laterally aligned zinc oxide nanorod arrays on a selected surface of the silicon substrate by a catalyst-free vapor solid process-a technique for growing nanocircuits, Phys. Chem. Chem. Phys. 15 (2013) 13532–13537.

[9] A. Arslan, E. Hür, S. Ilican, Y. Caglar, M. Caglar, Controlled growth of c-axis oriented ZnO nanorod array films by electrodeposition method and characterization, Spectrochim. Acta Part A: Mol. Biomol. Spectrosc. 128 (2014) 716–723.

[10] Y. Meng, Y. Lin, Y. Lin, Electrodeposition for the synthesis of ZnO nanorods modified by surface attachment with ZnO nanoparticles and their dye-sensitized solar cell applications, Ceram. Int. 40 (2014) 1693–1698.

[11] M. Rosina, P. Ferret, P.H. Jouneau, I.C. Robin, F. Levy, G. Feuillet, M. Lafossas, Morphology and growth mechanism of aligned ZnO nanorods grown by catalyst-free MOCVD, Microelectron. J. 40 (2009) 242–245.

[12] G.M. Fuge, T.M.S. Holmes, M.N.R. Ashfold, Ultrathin aligned ZnO nanorod arrays grown by a novel diffusive pulsed laser deposition method, Chem. Phys. Lett. 479 (2009) 125–127.

[13] M. Mehrabian, R. Azimirad, K. Mirabbaszadeh, H. Afarideh, M. Davoudian, UV detecting properties of hydrothermal synthesized ZnO nanorods, Phys. E: Low-Dimens. Syst. Nanostruct. 43 (2011) 1141–1145.

[14] M.H. Mamat, Z. Khusaimi, M.Z. Musa, M.Z. Sahdan, M. Rusop, Novel synthesis of aligned Zinc oxide nanorods on a glass substrate by sonicated sol–gel immersion, Mater. Lett. 64 (2010) 1211–1214.

[15] J. Han, Z. Liu, X. Zheng, K. Guo, X. Zhang, T. Hong, B. Wang, J. Liu, Trilaminar ZnO/ZnS/Sb2S3 nanotube arrays for efficient inorganic-organic hybrid solar cells, RSC Adv. 4 (2014) 23807–23814.

[16] N.K. Reddy, M. Devika, C.W. Tu, High-quality ZnO nanorod based flexible devices for electronic and biological applications, RSC Adv. 4 (2014) 37563–37568.

[17] M.H. Mamat, Z. Khusaimi, M.M. Zahidi, A.B. Suriani, Y.M. Siran, S.A. M. Rejab, A.J. Asis, S. Tahiruddin, S. Abdullah, M.R. Mahmood, Controllable Growth of Vertically Aligned Aluminum-Doped Zinc Oxide

Nanorod Arrays by Sonicated Sol–Gel Immersion Method depending on Precursor Solution Volumes, Jpn. J. Appl. Phys. 50 (2011) 06GH04.

[18] J.H. Huang, C.Y. Wang, C.P. Liu, W.H. Chu, Y.J. Chang, Large-area growth of vertically aligned ZnO pillars by radio-frequency magnetron sputtering, Appl. Phys. A: Mater. Sci. Process. 87 (2007) 749–753.

[19] B. Angadi, H.C. Park, H.W. Choi, J.W. Choi, W.K. Choi, Oxygen plasma treated epitaxial ZnO thin films for Schottky ultraviolet detection, J. Phys. D.: Appl. Phys. 40 (2007) 1422.

[20] S.P. Chang, R.W. Chuang, S.J. Chang, C.Y. Lu, Y.Z. Chiou, S.F. Hsieh, Surface HCl treatment in ZnO photoconductive sensors, Thin Solid Films 517 (2009) 5050–5053.

[21] H.W. Ra, R. Khan, J.T. Kim, B.R. Kang, K.H. Bai, Y.H. Im, Effects of surface modification of the individual ZnO nanowire with oxygen plasma treatment, Mater. Lett. 63 (2009) 2516–2519.

[22] A. Bera, D. Basak, Pd-nanoparticle-decorated ZnO nanowires: ultraviolet photosensitivity and photoluminescence properties, Nanotechnology 22 (2011) 265501.

[23] A. Bera, D. Basak, Photoluminescence and Photoconductivity of ZnS-Coated ZnO Nanowires, ACS Appl. Mater. Interfaces 2 (2010) 408–412.

[24] J.P. Kar, S.N. Das, J.H. Choi, Y.A. Lee, T.Y. Lee, J.M. Myoung, Fabrication of UV detectors based on ZnO nanowires using silicon microchannel, J. Cryst. Growth 311 (2009) 3305–3309.

[25] C.-H. Hsu, Y.-D. He, Electrical Properties of ZnO-Doped Nd($Co_{1/2}Ti_{1/2}$)O_3 Thin Films Prepared by RF Magnetron Sputtering, Jpn. J. Appl. Phys. 52 (2013) 01AC01.

[26] H. Zhu, J. Hüpkes, E. Bunte, S.M. Huang, Oxygen influence on sputtered high rate ZnO:Al films from dual rotatable ceramic targets, Applied Surface Science, 256, 2010, p. 4601–4605.

[27] S. Kim, J. Jeon, H.W. Kim, J.G. Lee, C. Lee, Influence of substrate temperature and oxygen/argon flow ratio on the electrical and optical properties of Ga-doped ZnO thin films prepared by rf magnetron sputtering, Cryst. Res. Technol. 41 (2006) 1194–1197.

[28] S. Shet, K.-S. Ahn, R. Nuggehalli, Y. Yan, J. Turner, M. Al-Jassim, Effects of substrate temperature and RF power on the formation of aligned nanorods in ZnO thin films, JOM 62 (2010) 25–30.

[29] T.L. Chou, W.Y. Wu, J.M. Ting, Sputter deposited ZnO nanowires/thin film structures on glass substrate, Thin Solid Films 518 (2009) 1553–1556.

[30] C.W. Hsu, T.C. Cheng, C.H. Yang, Y.L. Shen, J.S. Wu, S.Y. Wu, Effects of oxygen addition on physical properties of ZnO thin film grown by radio frequency reactive magnetron sputtering, J. Alloy. Compd. 509 (2011) 1774–1776.

[31] C.H. Ahn, Y.Y. Kim, S.W. Kang, B.H. Kong, S.K. Mohanta, H.K. Cho, J.H. Kim, H.S. Lee, Dependency of oxygen partial pressure on the characteristics of ZnO films grown by radio frequency magnetron sputtering, J. Mater. Sci.: Mater. Electron. 19 (2008) 744–748.

[32] K.B. Sundaram, A. Khan, Characterization and optimization of zinc oxide films by r.f. magnetron sputtering, Thin Solid Films 295 (1997) 87–91.

[33] X.C. Wang, X.M. Chen, B.H. Yang, Microstructure and optical properties of polycrystalline ZnO films sputtered under different oxygen flow rates, J. Alloy. Compd. 488 (2009) 232–237.

[34] J. Tauc, R. Grigorovici, A. Vancu, Optical Properties and Electronic Structure of Amorphous Germanium, Phys. Stat. Sol. 15 (1966) 627–637.

[35] E.A. Davis, N.F. Mott, electrical and transparent properties of amorphous semiconductor, Philos. Mag. 22 (1970) 903–920.

[36] S.A. Ansari, M.M. Khan, S. Kalathil, A. Nisar, J. Lee, M.H. Cho, Oxygen vacancy induced band gap narrowing of ZnO nanostructures by an electrochemically active biofilm, Nanoscale 5 (2013) 9238–9246.

[37] K. Jug, V.A. Tikhomirov, Influence of intrinsic defects on the properties of zinc oxide, J. Comput. Chem. 29 (2008) 2250–2254.

[38] L. Sun, W. Cheng, F. Lin, X. Ma, W. Shi, Changes of structure and optical energy gap induced by oxygen pressure during the deposition of ZnO films, Phys. B: Condens. Matter 381 (2006) 109–112.

[39] W. Daranfed, M.S. Aida, A. Hafdallah, H. Lekiket, Substrate temperature influence on ZnS thin films prepared by ultrasonic spray, Thin Solid Films 518 (2009) 1082–1084.

[40] B. Said, C. Foued, B. Boubaker, Z.L. Fatima, Influence of growth time on crystalline structure, conductivity and optical properties of ZnO thin films, J. Semicond. 34 (2013) 023001.

[41] V. Bhavanasi, C.B. Singh, D. Datta, V. Singh, K. Shahi, S. Kumar, Structural, optical and light scattering properties of post etched RF sputtered ZnO:Al thin films deposited at various substrate temperature, Optical Materials, 35, 2013, p. 1352–1359.

[42] S.H. Jeong, B.S. Kim, B.T. Lee, Photoluminescence dependence of ZnO films grown on Si(100) by radio-frequency magnetron sputtering on the growth ambient, Appl. Phys. Lett. 82 (2003) 2625–2627.

[43] Q.P. Wang, D.H. Zhang, Z.Y. Xue, X.J. Zhang, Mechanisms of green emission from ZnO films prepared by rf magnetron sputtering, Opt. Mater. 26 (2004) 23–26.

[44] Z.Y. Xue, D.H. Zhang, Q.P. Wang, J.H. Wang, The blue photoluminescence emitted from ZnO films deposited on glass substrate by rf magnetron sputtering, Appl. Surf. Sci. 195 (2002) 126–129.

[45] I.T. Tang, Y.C. Wang, W.C. Hwang, C.C. Hwang, N.C. Wu, M. P. Houng, Y.H. Wang, Investigation of piezoelectric ZnO film deposited on diamond like carbon coated onto Si substrate under different sputtering conditions, J. Cryst. Growth 252 (2003) 190–198.

[46] S.I. Inamdar, K.Y. Rajpure, High-performance metal–semiconductor–metal UV photodetector based on spray deposited ZnO thin films, J. Alloy. Compd. 595 (2014) 55–59.

[47] L.M. Wong, S.Y. Chiam, J.Q. Huang, S.J. Wang, J.S. Pan, W.K. Chim, Role of oxygen for highly conducting and transparent gallium-doped zinc oxide electrode deposited at room temperature, Appl. Phys. Lett. 98 (2011) 022106.

[48] Y.S. Chang, J.M. Ting, Growth of ZnO thin films and whiskers, Thin Solid Films 398–399 (2001) 29–34.

[49] E.M. Bachari, G. Baud, S. Ben Amor, M. Jacquet, Structural and optical properties of sputtered ZnO films, Thin Solid Films 348 (1999) 165–172.

[50] F. Urbach, The long-wavelength edge of photographic sensitivity and of the electronic absorption of solids, Phys. Rev. 92 (1953) 1324.

[51] J. Mass, P. Bhattacharya, R. Katiyar, Effect of high substrate temperature on Al-doped ZnO thin films grown by pulsed laser deposition, Mater. Sci. Eng.: B 103 (2003) 9–15.

[52] S.K. Panda, C. Jacob, Preparation of transparent ZnO thin films and their application in UV sensor devices, Solid-State Electron. 73 (2012) 44–50.

[53] H. Seo, L.R. Baker, A. Hervier, J. Kim, J.L. Whitten, G.A. Somorjai, Generation of highly n-type titanium oxide using plasma fluorine insertion, Nano Lett. 11 (2011) 751–756.

[54] R.C. Chang, S.Y. Chu, C.S. Hong, Y.T. Chuang, An investigation of preferred orientation of doped ZnO films on the 36° YX-LiTaO3 substrates and fabrications of Love-mode devices, Surf. Coat. Technol. 200 (2006) 3235–3240.

[55] T. Tsuji, M. Hirohashi, Influence of oxygen partial pressure on transparency and conductivity of RF sputtered Al-doped ZnO thin films, Appl. Surf. Sci. 157 (2000) 47–51.

[56] M.H. Mamat, M.I. Che Khalin, N.N.H. Nik Mohammad, Z. Khusaimi, N. D. Md Sin, S.S. Shariffudin, M. Mohamed Zahidi, M.R. Mahmood, Effects of annealing environments on the solution-grown, aligned aluminium-doped zinc oxide nanorod-array-based ultraviolet photoconductive sensor, J. Nanomater. 2012 (2012) 189279.

[57] J.H. Jun, H. Seong, K. Cho, B.-M. Moon, S. Kim, Ultraviolet photodetectors based on ZnO nanoparticles, Ceram. Int. 35 (2009) 2797–2801.

[58] S. Mridha, M. Nandi, A. Bhaumik, D. Basak, A novel and simple approach to enhance ultraviolet photosensitivity: activated-carbon-assisted growth of ZnO nanoparticles, Nanotechnology 19 (2008) 275705.

[59] K.P. Kim, D. Chang, S.K. Lim, S.K. Lee, H.K. Lyu, D.K. Hwang, Thermal annealing effects on the dynamic photoresponse properties of Al-doped ZnO nanowires network, Curr. Appl. Phys. 11 (2011) 1311–1314.

[60] Y.K. Su, S.M. Peng, L.W. Ji, C.Z. Wu, W.B. Cheng, C.H. Liu, Ultraviolet ZnO nanorod photosensors, Langmuir 26 (2010) 603–606.

[61] O. Lupan, G. Chai, L. Chow, G.A. Emelchenko, H. Heinrich, V. V. Ursaki, A.N. Gruzintsev, I.M. Tiginyanu, A.N. Redkin, Ultraviolet

photoconductive sensor based on single ZnO nanowire, Phys. Status Solidi (A) 207 (2010) 1735–1740.

[62] T. Ghosh, M. Dutta, S. Mridha, D. Basak, Effect of Cu doping in the structural, electrical, optical, and optoelectronic properties of sol–gel ZnO thin films, J. Electrochem. Soc. 156 (2009) H285–H289.

[63] M.H. Mamat, N.I. Ishak, Z. Khusaimi, M.M. Zahidi, M.H. Abdullah, S. Muhamad, N.D.M. Sin, M.R. Mahmood, Thickness-dependent characteristics of aluminium-doped zinc oxide nanorod-array-based, ultraviolet photoconductive sensors, Jpn. J. Appl. Phys. 51 (2012) 06FF03.

[64] P.S. Shewale, Y.S. Yu, Structural, surface morphological and UV photodetection properties of pulsed laser deposited Mg-doped ZnO nanorods: effect of growth time, J. Alloy. Compd. 654 (2016) 79–86.

[65] J. Cheng, Y. Zhang, R. Guo, ZnO microtube ultraviolet detectors, J. Cryst. Growth 310 (2008) 57–61.

[66] J.G. Ok, S.H. Tawfick, K.A. Juggernauth, K. Sun, Y. Zhang, A.J. Hart, Electrically addressable hybrid architectures of zinc oxide nanowires grown on aligned carbon nanotubes, Adv. Funct. Mater. 20 (2010) 2470–2480.

[67] A. Bera, D. Basak, Effect of surface capping with poly(vinyl alcohol) on the photocarrier relaxation of ZnO nanowires, ACS Appl. Mater. Interfaces 1 (2009) 2066–2070.

[68] M.H. Mamat, Z. Khusaimi, M.M. Zahidi, S.A. Bakar, M.Z. Yusop, M. Tanemura, M.R. Mahmood, Effects of aluminium doping and electrode distance on the performance of aligned zinc oxide nanorod array-based ultraviolet photoconductive sensors, Jpn. J. Appl. Phys. 51 (2012) 06FE04.

[69] Y. Jin, J. Wang, B. Sun, J.C. Blakesley, N.C. Greenham, Solution-Processed Ultraviolet Photodetectors Based on Colloidal ZnO Nanoparticles, Nano Lett. 8 (2008) 1649–1653.

[70] I.C. Yao, T.Y. Tseng, P. Lin, ZnO nanorods grown on polymer substrates as UV photodetectors, Sens. Actuators A: Phys. 178 (2012) 26–31.